Nuclear Inst. and Methods in Physics Research, A 1028 (2022) 166328

Contents lists available at ScienceDirect

Nuclear Inst. and Methods in Physics Research, A

journal homepage: www.elsevier.com/locate/nima

Pulse characteristics of CLYC and piled-up neutron–gamma discrimination using a convolutional neural network

Jifeng Han [a], Jialiang Zhu [b], Zhonghai Wang [a], Guofeng Qu [a,*], Xingquan Liu [a], Weiping Lin [a], Zixu Xu [a], Yu Huang [a], Min Yan [a], Xin Zhang [a], Lei Chen [a]

[a] Key Laboratory of Radiation Physics and Technology of the Ministry of Education, Institute of Nuclear Science and Technology, Sichuan University, Chengdu, 610064, China

[b] Science and Technology on Reactor System Design Technology Laboratory, Chengdu, 610213, China

ARTICLE INFO

Keywords:
$Cs_2LiYCl_6:Ce^{3+}$ scintillator
Pulse shape discrimination
Neutron–gamma identification
Fully connected neural network
Convolutional neural network

ABSTRACT

A method of describing the characteristics of Cs_2 $LiYCl_6$ scintillator pulses is proposed by fitting all individual pulses with multiple exponential functions. Simulated pulses under very high counting rates (e.g., 2–40 Million counts per second) are generated by sampling from fitted parameter distributions, which include the non piled-up neutron (n) and gamma (g) pulses as well as piled-up gamma + neutron (g + n), neutron + gamma (n + g), neutron + neutron (n + n), and gamma + gamma (g + g) pulses. A fully connected neural network (FCNN) model can discriminate n and g signals clearly and demonstrates a discrimination performance similar to the traditional charge comparison method. A model trained with experimental data demonstrated very good prediction accuracy on simulated data, and a model trained with simulated data demonstrated good prediction accuracy on experimental data as well, indicating all characteristic of CLYC had been simulated. A convolutional neural network (CNN) model could discriminate between the six pulse types more effectively than a FCNN model, producing a discrimination error lower than 0.22% for n, g, n + g, and n + n pulses, and an error lower than 3.61% for g + g and g + n pulses. These results indicate that a CNN model is very suitable for complicated n–g discrimination under a piled-up condition.

1. Introduction

A $Cs_2LiYCl_6:Ce^{3+}$ (CLYC) scintillator can be used as an effective nuclear detector for both gamma and neutron detection, providing much better energy resolution (about 5% @ 662 keV) than an NaI detector for gamma rays [1], acceptable detection efficiency for thermal/cold neutrons when enriched ^{6}Li (normally 95%) is used in the detector, and a good pulse shape discrimination (PSD) for neutrons and gammas [2]. The PSD method is widely used to discriminate between neutron and gamma signals in nuclear applications (e.g., safeguards [3] and homeland security [4]). Several methods have been proposed to apply the PSD and evaluate the performance of a nuclear detector. For example, the charge comparison method provides valuable discrimination between non-piled-up pulses and figure-of-merit (FOM) is widely used to evaluate the discrimination performance of the detector [5,6]. Moreover, many machine learning methods (e.g., support vector learning [7], artificial neural networks [8–10], principal component analysis [11], recurrent neural networks [12], triangular and trapezoidal filters [13], and convolutional neural networks (CNN) [14]) have been introduced into PSD analysis and proven to improve the discrimination performance.

The pulses might be piled-up due to high counting rates, which greatly change the structures of pulses [5] and render the traditional charge comparison methods invalid. A fully connected neural network (FCNN) and a recurrent neural network was used to perform the PSD of piled-up pulses for organic scintillators [12], reporting fractions of incorrectly classified neutron, gamma, and piled-up pulses as 1%, 1.8%, and 0.6%, respectively, at a high counting rate of 100 thousand counts per second (kcps). Triangular and trapezoidal filters were used for PSD of CLYC at 375 kcps, adequately identifying neutrons and gammas [13].

Most PSD methods have been applied to scintillators (such as BC-501 [8,9], EJ-301 [10], CLYC [13], and ^{6}Li F:ZnS(Ag) [14]) at moderate counting rates of several hundreds of kcps, while the studies conducted at very high counting rates of several thousand kcps remain scarce. On the other hand, CNN have proven sufficiently powerful for applications in many fields, such as computer vision, image identification, and computerized electrocardiogram interpretation [15,16]. J. Griffiths used a CNN to discriminate between neutrons and gammas, proving the network's flexibility and ability to extract combined features [14].

* Corresponding author.
E-mail address: quguofeng@scu.edu.cn (G. Qu).

https://doi.org/10.1016/j.nima.2022.166328
Received 25 May 2021; Received in revised form 19 October 2021; Accepted 4 January 2022
Available online 12 January 2022
0168-9002/

In this work, the PSD performance of CLYC is studied by comparing the discrimination accuracy of traditional charge comparison method, a FCNN, and a CNN. First, the signal characteristics of approximately 36,000 CLYC scintillator pulses are analyzed and are then fitted with a multi-exponent function to analyze the parameter distributions. Second, artificial CLYC pulses under very high counting rates, about 2–40 Million counts per second (Mcps), are simulated by sampling from the former parameter distributions. Finally, a FCNN and an one-dimensional CNN network are designed to discriminate these pulses and the discrimination accuracy and error of the networks are compared and discussed.

2. Experiment setup and data analysis method

The pulses were generated from one 10 mm × 10 mm × 10 mm CLYC scintillator (using ^{6}Li enrichment of 95%) coupled with a Hamamatsu R6231-100 photomultiplier tube (PMT) applied at a high voltage of 1000 V. PMT pulses were acquired using a high-speed LeCroy oscilloscope with a sampling rate of 1.25 G samples per second and a trigger threshold of −12 mV. For convenience, the reversed positive pulses were used for analysis in this study. Gamma pulses were acquired by detecting the 59.6 keV X-ray of a ^{241}Am source, whose activity was about 5 μCi, while the neutron and associated gamma pulses were acquired using an Am–Be source with a neutron emission rate of approximately 10,000 n/s. The CLYC detector was placed close to the source (about 0.4 m for Am–Be source, and 2 mm for ^{241}Am source) to increase the acquisition efficiency. The pulse differences between neutron and gamma signals are presented in Section 2.1.

2.1. Signal characteristics of CLYC

Three typical pulse types were found by the CLYC; they are shown in Fig. 1 as Type_1, Type_2, and Type_3. The Type_3 pulses were very narrow, with a full width at half maximum (FWHM) of approximately 15 ns, and could be fitted with a Landau function, these pulses were assigned as noise pulses from the PMT. The pulse widths of Type_1 were much wider than those of Type_2, indicating the greater significance of the faster component in Type_2.

The percentage of collected pulses were significantly different for ^{241}Am and Am–Be sources, as shown in Table 1. Excluding Type_3 pulses (PMT noise), mainly Type_2 pulses were found for ^{241}Am source. Since ^{241}Am can only generate gamma rays but not neutrons, it can be concluded that Type_2 pulses were generated by gamma rays. Conversely, both Type_1 and Type_2 pulses were found for the Am–Be source, because both neutron and associated gamma particles can be emitted from the source. The shape of the Type_2 pulses originating from Am–Be source was identical to the ^{241}Am source, indicating that Type_2 pulses were generated by gamma rays while Type_1 pulses were generated by neutrons. When a 20-mm-thick lead brick was inserted between the Am–Be source and the CLYC detector, the percentage of Type_2 pulses decreased accordingly. This confirmed that Type_2 pulses were generated by gammas because the brick shielded more gammas than neutrons. This is consistent with previous studies [1,2,14] that reported neutrons generating wider signals than gammas. About 1.8% of Type_1 pulses were found during the ^{241}Am data acquisition process and were assigned to background or cosmic ray neutrons. The width of the neutron pulse (Type_1) is wider than that of the gamma pulse (Type_2), and can be discriminated using the PSD method.

2.2. Fitting of the experimental pulses

CLYC has four emission mechanisms under gamma ray radiation [2,17,18]: the ultrafast core-to-valence luminescence (CVL), the fast direct electron–hole capture by Ce^{3+}, the intermediate speed binary Vk formation and electron diffusion, and the slow emission by Ce^{3+} and self-trapped excitation. The CVL component, observed for Cs_2LiYCl_6:Ce^{3+} but not for Cs_2LiYBr_6:Ce^{3+} [18], makes CLYC convenient for gamma and neutron discrimination. To describe all four components, Type_1 and Type_2 pulses were fitted with Eq. (1).

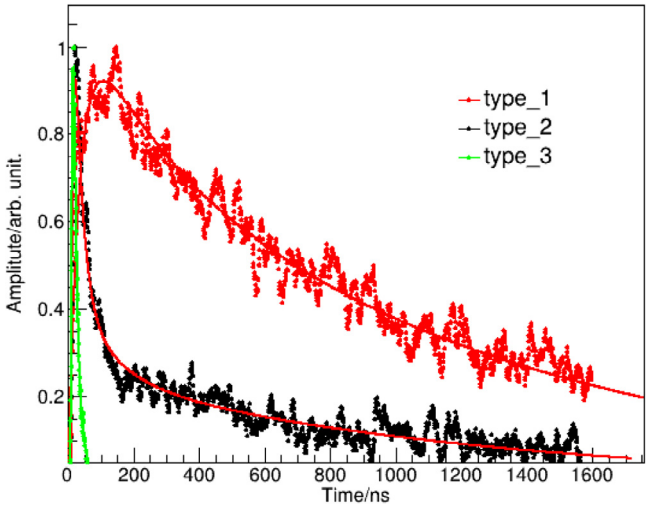

Fig. 1. Typical pulse types generated by the CLYC detector.

Table 1
Fraction distribution of three pulse types.

	^{241}Am (%)	Am–Be (%)
Type_1	1.8	52.1
Type_2	49.3	29.5
Type_3	48.9	18.4

$$Y = -A_1 e^{-\frac{t}{\tau_1}} + A_2 e^{-\frac{t}{\tau_2}} + A_3 e^{-\frac{t}{\tau_3}} + A_4 e^{-\frac{t}{\tau_4}} \quad (1)$$

Four exponential functions were included in Eq. (1), the first relates to the rising edge, and the following three relate to the falling edges. Eight parameters are used in Eq. (1): four time-constant parameters (τ) and four gain parameters (A).

As shown in Fig. 1, there is periodic noise on the falling edge that contributes greatly to the sum calculation of the squared deviations, rendering the least square fitting difficult to converge. This noise can be neutralized by averaging numerous scaled pulses, making the fitting much easier [2,17]. In this study, 2000 scaled pulses were used to calculate the average pulses for Type_2 (gamma) and Type_1 (neutron), as shown in Fig. 2(a) and (b), respectively. It was found that the noise decreased greatly for averaged pulses, and can be fitted much easily with Eq. (1).

The ROOT package, developed by CERN [19], was used to fit the averaged pulses. Preset initial parameter values and limits are important for the successful fitting of Eq. (1). The fitted curves for gamma and neutron pulses are shown in Fig. 2, which overlap with the data well. In Fig. 2(a), the fitted peak is not as sharp as its data; this can be improved by deleting several data points at the onset of the pulse. For example, deleting the first five points increases the fitted peak amplitude from 0.93 to 0.98 (the maximum data peak is 1.00) and decreases the χ^2/ndf from 0.134/1797 to 0.018/1792. However, it is found that such deletions are only usable for the fitting of averaged pulses; they become impractical for an individual pulse fitting where large noise is superimposed on the pulses. Several averaged pulses were calculated and fitted, producing fitted parameters that differed slightly with a maximum variation of approximately 2%. The mean values for the four fitted time constants are shown in Table 2. The time constants of the gamma pulses were much smaller than those of neutron pulses, indicating that gamma pulses increase faster at the rising edge and decrease faster at the falling edge. There is no fast component

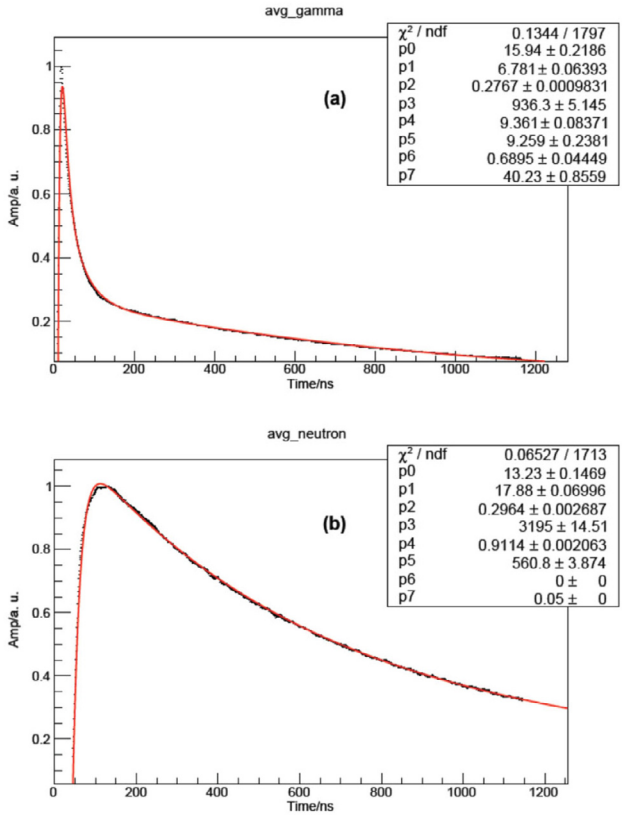

Fig. 2. Average pulses fitted with Eq. (1): (a) gamma and (b) neutron.

Table 2
Fitted Time Constants for Average Pulses.

	τ_1 (ns)	τ_2 (ns)	τ_3 (ns)	τ_4 (ns)
neutron	17.8 ± 0.02	3193 ± 10	570 ± 10	–
gamma	7.35 ± 0.05	918 ± 10	10.2 ± 0.02	43 ± 0.5

at the falling edge of the neutron signal, which can be used for the discrimination of neutron and gamma pulses.

The eight parameters in Eq. (1) introduces considerable freedom, and the fitting might converge to different parameters when different preset values are used. The accurate time constant calculation are not considered as a key point of this study, we did not considerably focus on the accurate fitting. The fitted time constants differed from those reported in [2] but were close to those reported in [17]. These value differences may have been caused by the CLYC manufacturing process.

In this work, approximately 36,000 individual pulses were fitted and the distributions of the fitted parameters were analyzed to understand the pulse characteristics of CLYC. To simplify the fitting, the four time constants (τ_1, τ_2, τ_3, and τ_4) in Eq. (1) were fixed to the mean value of the average pulses shown in Table 2 and the four gain parameters (A_1, A_2, A_3, and A_4) were fitted and analyzed further. The gain parameters were found to follow a Gaussian distribution; the A_1 and A_2 parameters for gamma and neutron pulses, respectively, are shown in Fig. 3 and were fitted with a Gaussian function. The fitted parameters are summarized in Table 3. By using data from Tables II and III, the CLYC pulse characteristics can be described very well with Eq. (1).

The pulses were scaled to a maximum value of 1.00 prior to fitting. The maximum amplitude distributions of neutron and gamma pulses from Am–Be sources are shown in Fig. 4(a) and (c), respectively. Data in Fig. 4(a) were fitted with a Gaussian function, whereas data in Fig. 4(c) were fitted with a Landau function. The fitted parameters

Table 3
Gain Parameters for Neutron and Gamma Pulses.

	A_1	A_2	A_3	A_4
neutron	1.66 ± 0.16	0.35 ± 0.03	0.62 ± 0.04	–
gamma	15.38 ± 4.16	0.30 ± 0.03	6.69 ± 2.34	0.93 ± 0.18

Table 4
Peak and Noise Parameters for Neutron and Gamma.

	Pulse_amplitude	Noise_cycle	nos_amp_ratio
neutron	16.9 ± 1.0	10 ± 7	3.64%
gamma	20.5 ± 3.5	10 ± 7	6.63%

are shown in the "Pulse_Amplitude" column of Table 4. The energy resolution of CLYC for neutrons can be calculated using the sigma relative to the mean value in Fig. 4(a), which is 5.8%. The resolution was bad because of the larger pulse noise. An energy resolution of 3.5% was acquired by using total integration rather than the maximum pulse amplitude, which is slightly worse than the value of 2.9% reported in [1]. This may be attributed to the low vertical resolution (eight bits) of the oscilloscope.

There was periodic noise on the falling edge of the CLYC pulse (Fig. 1) that could be extracted by subtracting data with the fitted curve. The noise can be described using noise cycle and noise amplitude. The noise cycle followed a Gaussian distribution, where the mean and sigma values of the Gaussian function were 10 ns and 7 ns, respectively. The noise amplitude was proportional to the pulse amplitude, and the relative ratios of noise amplitude versus pulse amplitude (nos_amp_ratio) for neutron and gamma are shown in Fig. 4(b) and (d), respectively. Both ratios were fitted with a Gaussian function, and the sigma values were 3.64% and 6.63%, respectively. The noise in the neutron signals was much larger than that of the gammas; the noise parameters are summarized in Table 4.

2.3. CLYC pulse simulation

By sampling parameters from distributions shown in Tables 2, 3, and 4, the simulated signals can be generated randomly. It was important to consider the correlation between the four gain parameters to ensure successful sampling. For gamma pulses, gain parameters A_1, A_2, and A_4 were correlated with A_3 with correlation coefficients of 0.895, −0.389, and −0.746, respectively. For the neutrons, gain parameters A_1 and A_2 were correlated with A_3 with correlation coefficients of 0.454 and −0.334, respectively.

By adding the second pulse onto the first pulse, piled-up pulses could be generated. The time interval between the two pulse peaks was set to be randomly distributed within [25, 500] ns, and the counting rate was about 2–40 Mcps. When the time interval was shorter than 25 ns, the two pulses merged together to form one pulse rather than two piled-up pulses. When the time interval was longer than 500 ns, it was easier to discriminate using the charge comparison method discussed in Section 3.1. The information within 500 ns after each pulse peak was sufficient to distinguish neutrons from gammas, yet it was much more challenging to discriminate given a time interval shorter than 500 ns. Six types of typical simulated pulses are shown in Fig. 5: the non-piled-up gamma and neutron pulses, and the piled-up pulses of gamma + neutron (g + n), neutron + gamma (n + g), neutron + neutron (n + n), and gamma + gamma (g + g).

Under such a high counting rate, three or more pulses might be piled-up in a single detection window. The detailed discrimination of these three ordered or higher piled-up pulse types are not considered in this study because there are too many types. For example, three piled signals produce eight types (e.g., n + n + g) and four piled signals possess 16 types (e.g., n + n + g + n). In this case, it is recommended to identify highly piled-up signals using other methods during data processing and not to perform further discrimination. There are many

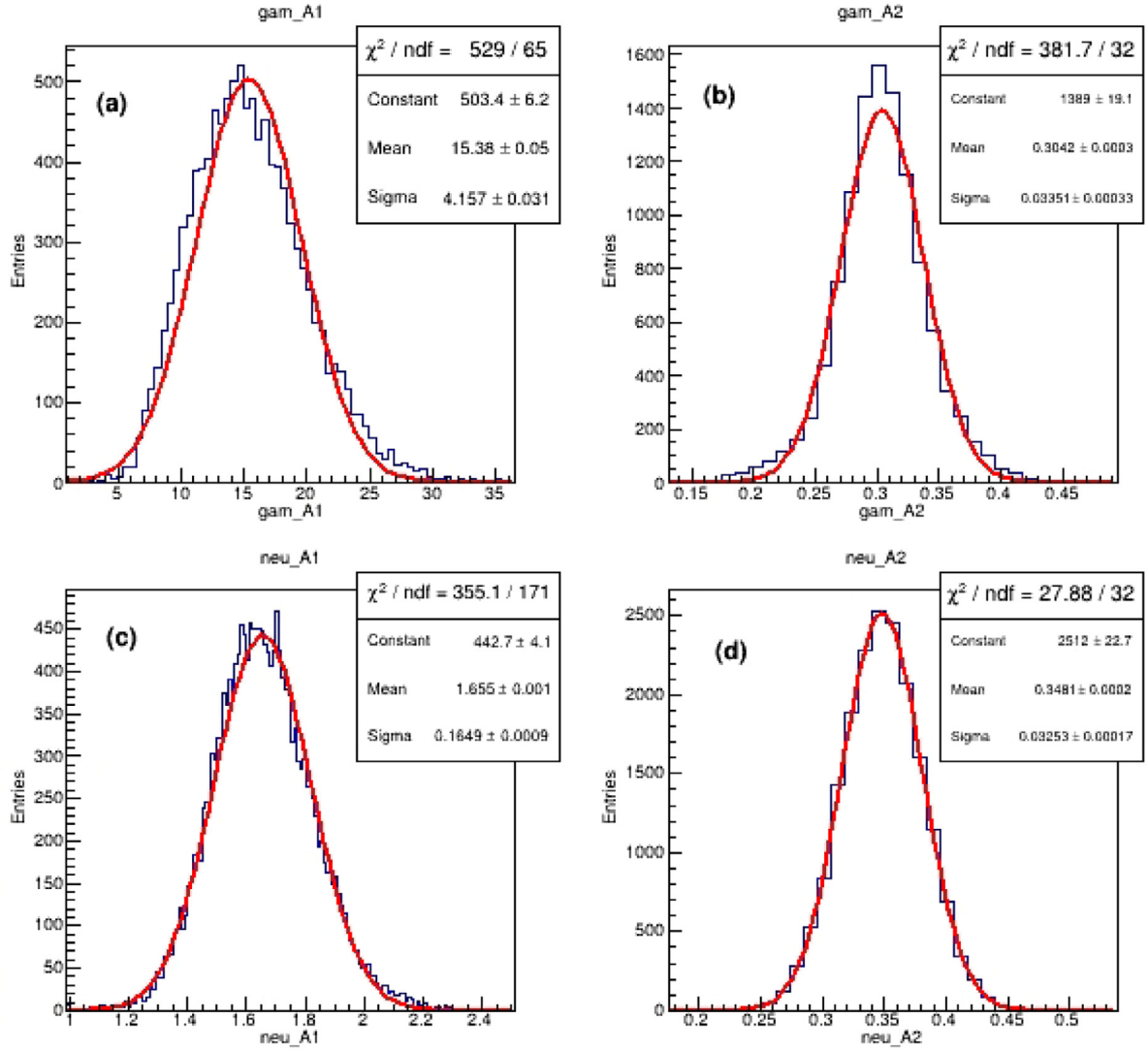

Fig. 3. Gain parameter distributions: (a) gamma pulse A_1, (b) gamma pulse A_2, (c) neutron pulse A_1, and (d) neutron pulse A_2.

methods for determining the number of peaks inside a detection window, an effective method is to calculate the number of rising edges within the window. This is because the rising edge is faster for both neutron and gamma, which induce significant peaks in the deviation signal of the pulse and render the identification much easier. The key point is to decrease the noise of the pulse, which might cause trouble during peak searching. A possible method is using the fast Fourier transform filter to convert the signal into a frequency domain, discard the higher frequency (noise of the pulse), and transform the remainder back into a time domain for further peak searching.

3. Neutron–gamma discrimination

3.1. Neutron–gamma discrimination using the charge comparison method

The shapes of gamma and neutron pulses are different (Fig. 2) and can be discriminated using the traditional charge comparison method. As shown in Table 2, the main difference between gamma and neutron pulses is the pulse width, or the presence of fast components on the falling edge with the time constants of 10 and 43 ns. A discrimination variable R_psd, shown in Eq. (2), can be defined to determine if a signal is a gamma or a neutron [20,21]. In Eq. (2), t_0 is the peak time of the pulse, the numerator is the integration of the pulse from t_0 to $t_0 + t_1$, and the denominator is the integration of the pulse from t_0 to $t_0 + t_2$. The values of t_1 and t_2 are optimized to ensure optimal discrimination performance ($t_1 = 24$ ns and $t_2 = 500$ ns).

$$R\_psd = \frac{\int_{t0}^{t0+t1} f(t)\,dt}{\int_{t0}^{t0+t2} f(t)\,dt} \tag{2}$$

The distribution of R_psd is shown in Fig. 6, where two discrete peaks are clearly shown. The first peak is due to neutron pulses with R_psd values <0.09, while the second peak is due to gamma pulses with R_psd values >0.09.

The discrimination performance can be described with FOM, as defined in Eq. (3), where the numerator is the separation between the neutron and gamma peaks, while the denominator is the sum of the FWHM for neutron and gamma peaks. The FOM value was calculated to be 2.30 from the fit results in Fig. 6, where about 5e-5 in one gamma might be mislabeled as neutron. It can be concluded that CLYC is able to discriminate neutron and gamma pulses with high accuracy. The FOM value in this manuscript is consistent with values of about 4.2–1.8 (2.8@20 °C) [2], about 0.85–1.8 [17], and 2.4 [22]. The integration window differs in the literature cited above, and it is reported that the method still works when the rising edge is included in the window [23].

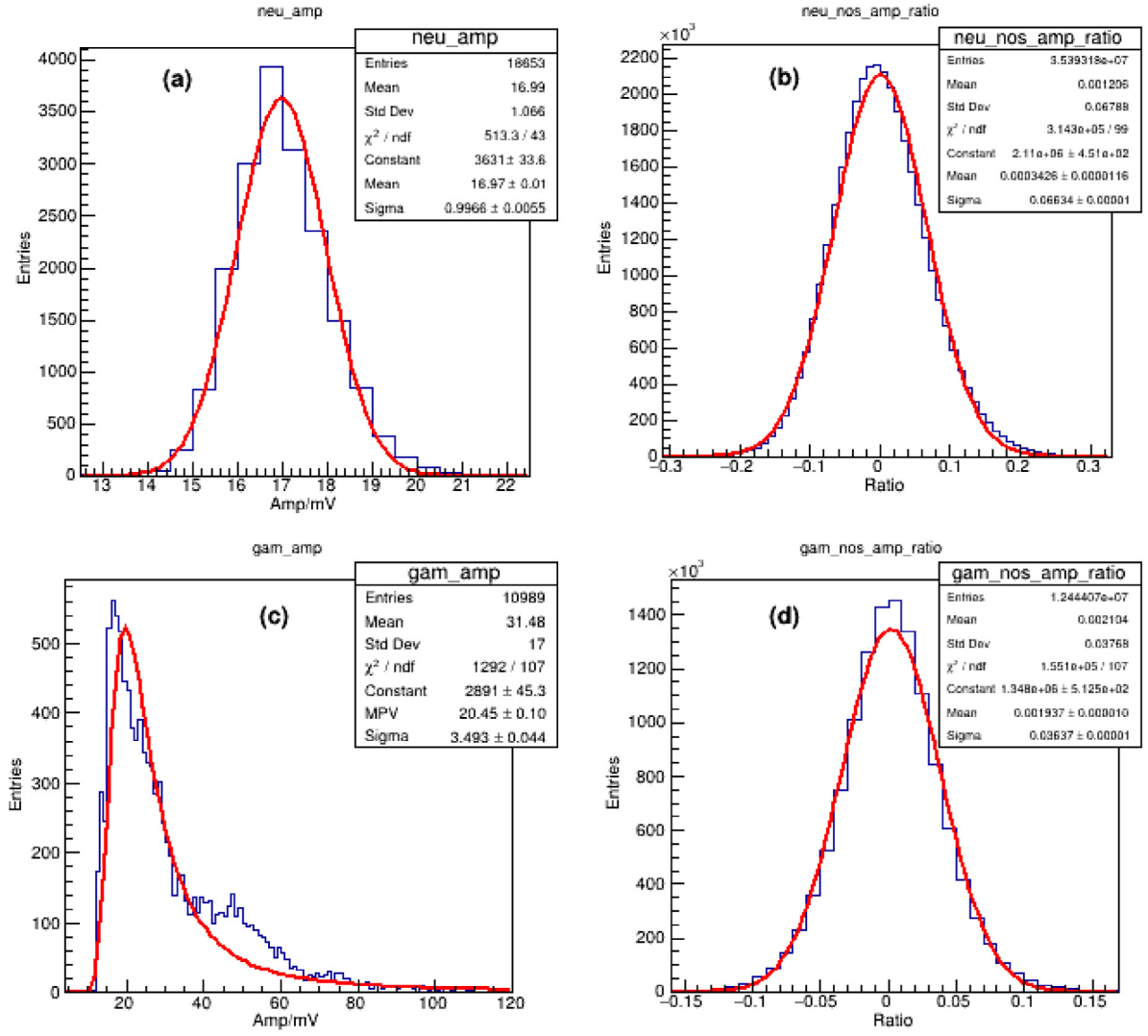

Fig. 4. Pulse maximum amplitude distribution: (a) neutron pulse amplitude distribution, (b) relative ratio of noise amplitude on falling edge for neutron (c) gamma amplitude distribution and (d) relative ratio of noise amplitude on falling edge for gamma.

That indicates the PSD method was not significantly sensitive to the integration window once the peak area was included.

$$FOM = \frac{\mu_\gamma - \mu_n}{FWHM_\gamma + FWHM_n} \tag{3}$$

3.2. Neutron–gamma discrimination using a FCNN model

A FCNN model (Model_ng), based on the Tensorflow2.0 and Keras2.2 packages developed by Google [24], was generated to discriminate between neutrons and gammas. Model_ng comprised two fully connected inner layers whose shapes were 200 and 20, respectively, and used the "ReLU" activation functions for both layers. The input layer of Model_ng comprised the full signal pulses comprising 2000 data points. The output layer of the model was a prediction possibility within [0, 1] using the "sigmoid" activation function. The label was set to one for neutron pulses, and zero for gamma pulses during training. Thus, the pulse was predicted to be a neutron for values close to one and a gamma for values close to zero during testing. The loss function used was "binary_crossentropy", and the optimizer was "Adam". In total, 404,241 trainable parameters existed in the network.

The dataset had about 36,000 signal pulses (about 60% were neutron pulses) that were divided into a train_set (80%) and test_set (20%). The train_set used 80% of its pulses for model training and the remaining 20% for validation during the training. The model accuracy and loss during training are shown in Fig. 7(a) and (b), respectively, with the validation accuracy and loss are estimated to be 99.95% and 1.2e−4, respectively, after 40 epochs. When using the trained model for performing predictions on the test_set, the test accuracy and loss were 100% and 1.7e−5, respectively. These results indicated that the neutral network model is very effective at neutron–gamma discrimination, performing similarly to the traditional FOM methods.

3.3. Simulated pulse validation

Model_ng was used to confirm if the simulated signals were similar to experimental signals. When Model_ng was trained using the experimental data for predicting the simulated data, its accuracy on simulated neutron and gamma pulses was 100% and 99.23%, respectively. When Model_ng was trained using simulated data and used to predict the experimental data, the accuracy on experimental neutron and gamma pulses was 99.93% and 99.65%, respectively. These results indicate that simulated pulses can accurately represent experimental pulses and that all CLYC characteristics were successfully simulated.

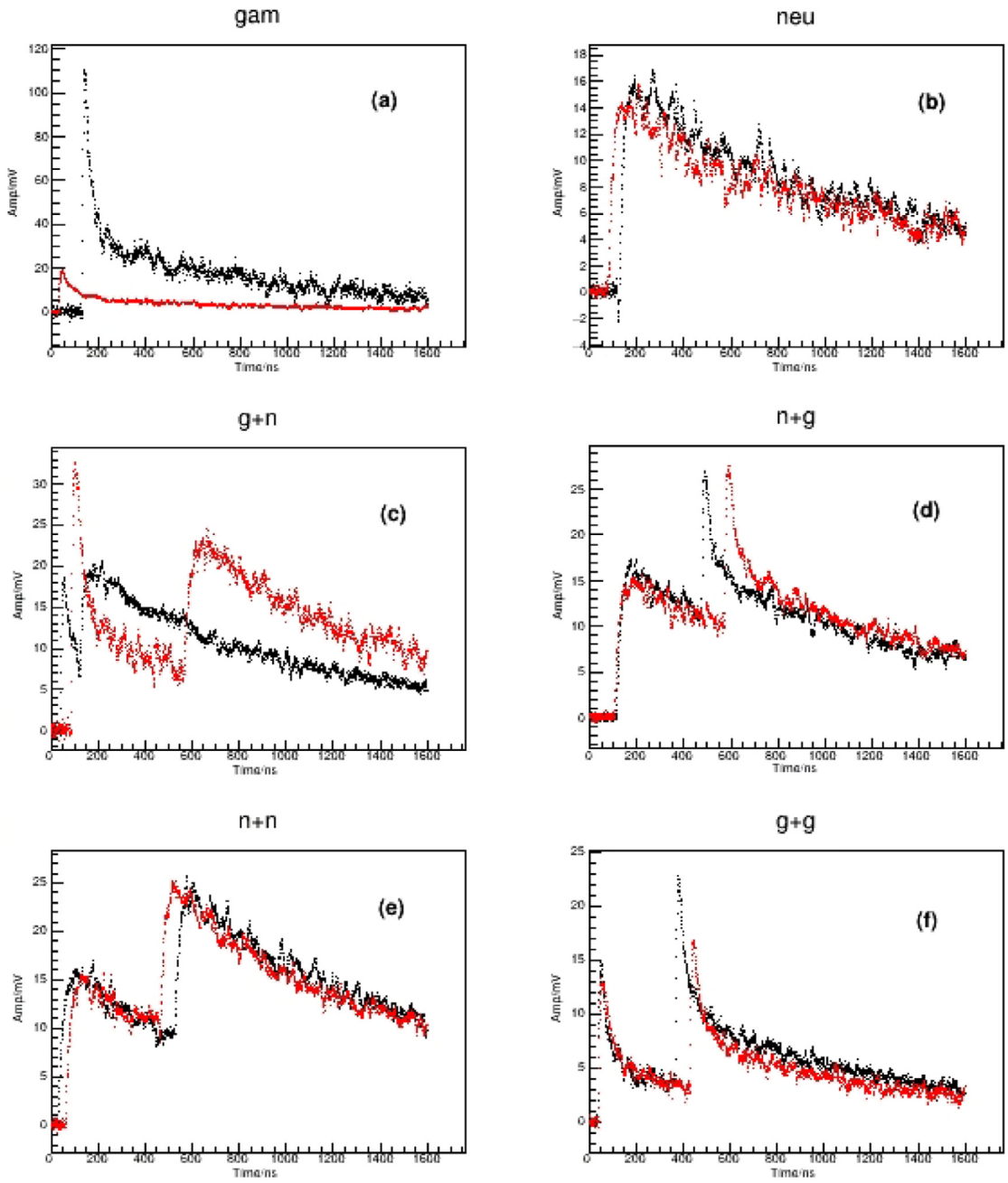

Fig. 5. Simulated signals: (a) g, (b) n, (c) g + n, (d) n + g, (e) n + n, and (f) g + g.

3.4. Piled-up pulse discrimination

The charge comparison method is only applicable to non-piled-up signals, whereas a neural network is able to discriminate between all six types of pulse types shown in Fig. 5. A FCNN model (Model_FCNN) and a CNN model (Model_CNN), based on the Tensorflow2 and Keras2 packages, were built to perform the discrimination. The two network structures are shown in Fig. 8. The structure of Model_FCNN was similar to Model_ng in Section 3.2, which includes two hidden layers; however, the output was a prediction of one out of the six possible pulse types. The structure of Model_CNN comprised six convolutional sections and one linear output layer that were also able to predict one of six pulse types. For each convolutional section, the Conv1D layer, Batch Normalization layer, "ReLU" activation function, and MaxPooling1D were applied. There were 404,346 parameters for Model_FCNN, while only 4686 parameters existed for Model_CNN. Although the structure of Model_CNN was much more complicated, it possessed only 11% of the parameters of Model_FCNN, making it more suitable for discrimination given similar performance.

About 60,000 simulated signals (10,000 for each signal type) and 16,000 detector signals (~60% neutron signals) were used to train the model. Another 60,000 simulated signals (10,000 for each signal type) and 20,000 detector signals (~60% neutron signals) were used for testing. Both models were trained and tested using the same dataset, and the training was stable after 80 epochs. The predicted accuracy and loss values obtained using the test data were 98.75% and 0.048, respectively, for Model_FCNN, while the corresponding values were 99.34% and 0.0286 for Model_CNN. The discrimination errors in case

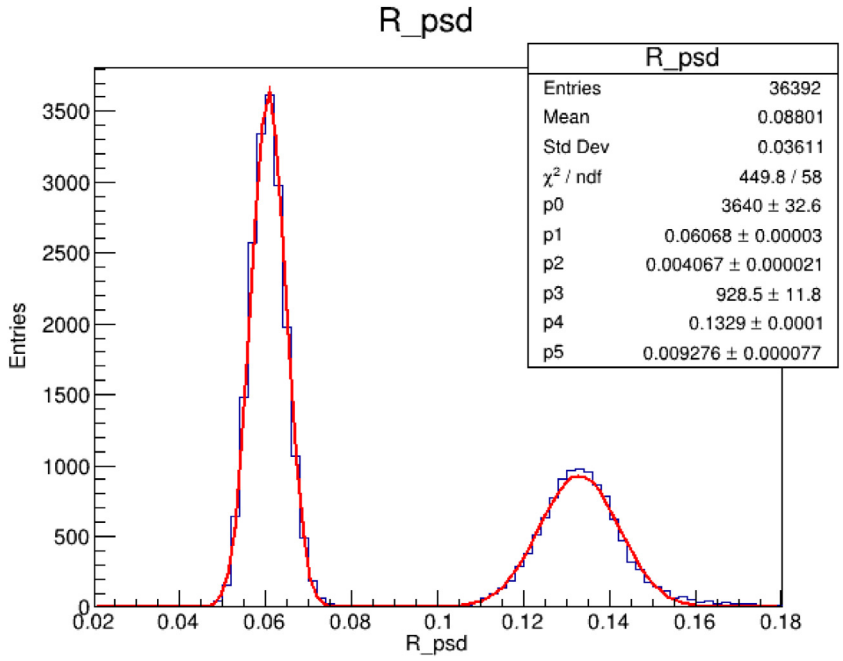

Fig. 6. Discrimination variable distribution.

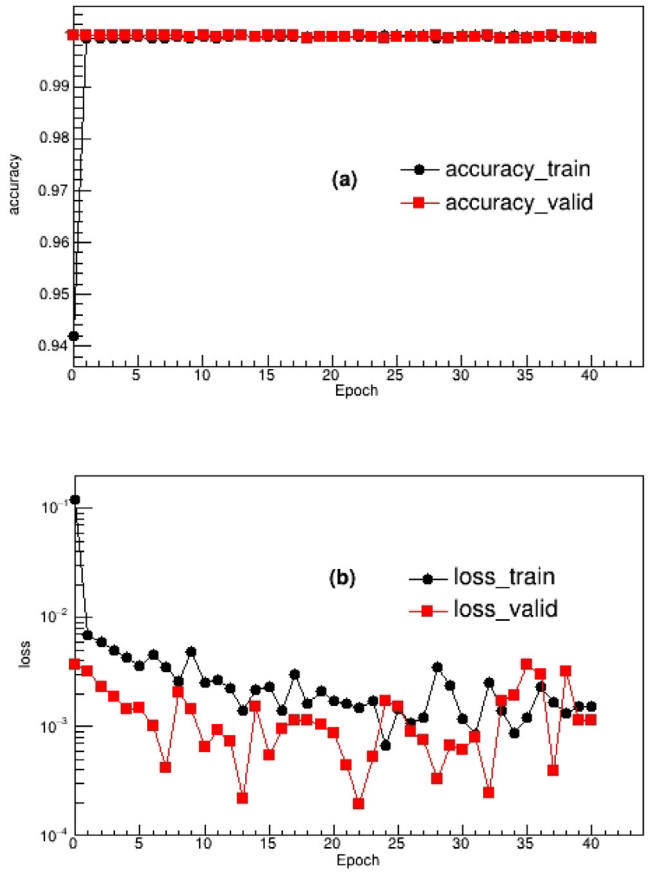

Fig. 7. Model measurements during training: (a) accuracy and (b) loss.

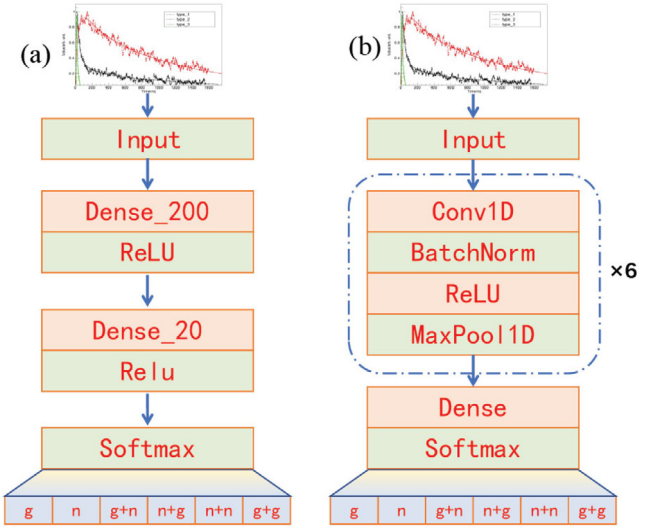

Fig. 8. Neural network structures: (a) Model_FCNN, (b) Model_CNN.

of the individual pulse types are shown in Table 5 for both models. Model_CNN was found to have a much lower discrimination error in all six pulse types, indicating that its performance was much better than that of Model_FCNN. The discrimination error for Model_CNN was less than 0.22% for g, n, n + g, and n + n pulses as well as less than 3.61% for g + g and g + n pulses; these results were much better than those reported in [17]. Thus, a CNN model is more suitable for conducting a complicated neutron–gamma discrimination under piled-up conditions, which require fewer parameters and possess better discrimination accuracy.

The discrimination confusion matrices for the six pulse types are shown in Fig. 9. For Model_CNN, g + g had largest discrimination error of 3.61% and 90% of its incorrectly discriminated pulses were mispredicted as gammas because the gamma pulse is narrow and a piled gamma might be mistaken as noise when the peak amplitude is small. As for g + n, about 77% of the incorrectly discriminated pulses were mispredicted as gammas because piled neutrons would make g +

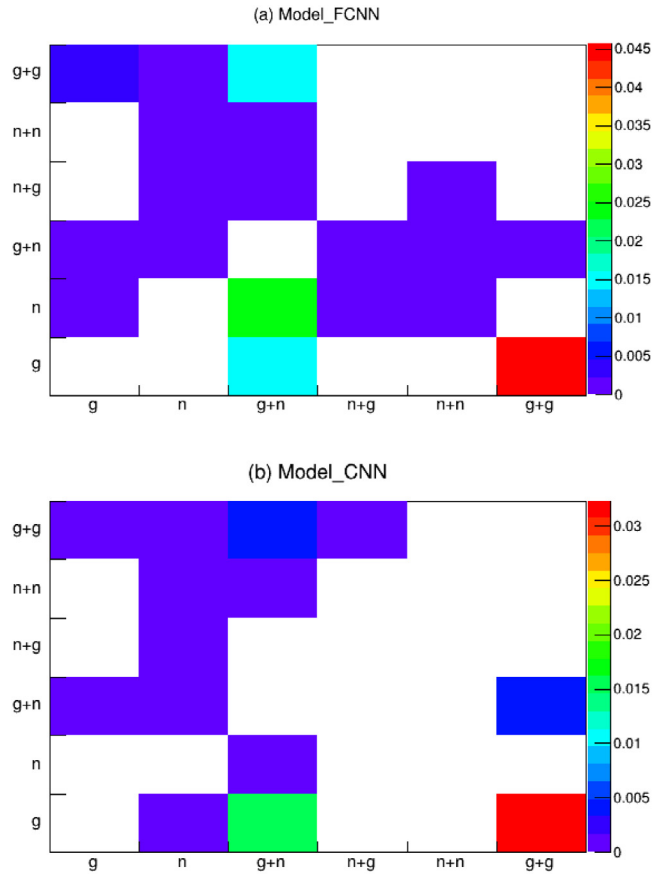

Fig. 9. Discrimination confusion matrices: (a) Model_FCNN and (b) Model_CNN.

Table 5
Neural network discrimination errors.

	g	n	g + n	n + g	n + n	g + g
Model_FCNN	0.47%	0.42%	5.49%	0.13%	0.07%	3.87%
Model_CNN	0.16%	0.22%	1.94%	0.01%	0.00%	3.61%

n resemble a gamma given a smaller peak amplitude of the piled-up neutrons.

4. Conclusion

Simulated signals under very high counting rates were generated by analyzing the characteristics of CLYC scintillator pulses. The neural network model can discriminate between neutrons and gammas effectively. It was found that a network model trained by experimental data had very good predication accuracy on simulated data, while a model trained by simulated data had good predication accuracy on experimental data, indicating all characteristic of CLYC had been simulated. A CNN model was used to perform the complicated discrimination of piled-up and non-piled-up pulses, achieving better accuracy than a FCNN model despite having only 11% of the parameters. These results indicated that a CNN model is more suitable for complicated neutron–gamma discrimination under high counting rates.

CRediT authorship contribution statement

Jifeng Han: Conceptualization, Methodology, Software, Writing – original draft, Writing – review & editing. **Jialiang Zhu:** Investigation. **Zhonghai Wang:** Data curation, Investigation. **Guofeng Qu:** Investigation, Writing – review & editing. **Xingquan Liu:** Investigation. **Weiping Lin:** Investigation. **Zixu Xu:** Investigation. **Yu Huang:** Investigation. **Min Yan:** Investigation. **Xin Zhang:** Investigation. **Lei Chen:** Investigation.

Declaration of competing interest

The authors declare that they have no known competing financial interests or personal relationships that could have appeared to influence the work reported in this paper.

Acknowledgments

This work was supported by National Natural Science Foundation of China (11575121), and the Fundamental Research Funds for the Central Universities, China.

References

[1] J. Glodo, W.M. Higgins, E.V.D. van Loef, K.S. Shah, Scintillation properties of 1 inch Cs_2LiYCl_6:Ce crystals, IEEE Trans. Nucl. Sci. 55 (3) (2008) 1206–1209.
[2] B.S. Budden, L.C. Stonehill, J.R. Terry, A.V. Klimenko, J.O. Perry, Characterization and investigation of the thermal dependence of Cs2LiYCl6:Ce3+ (CLYC) waveforms, IEEE Trans. Nucl. Sci. 60 (2) (2013) 946–951.
[3] A. Di Fulvio, T.H. Shin, T. Jordan, C. Sosa, M.L. Ruch, S.D. Clarke, D.L. Chichester, S.A. Pozzi, Passive assay of plutonium metal plates using a fast-neutron multiplicity counter, Nucl. Instrum. Methods Phys. Res. A 855 (2017) 92–101.
[4] A. Danagoulian, W. Bertozzi, C.L.H. Hicks Jr., A.V. Klimenko, S.E. Korbly, R.J. Ledoux, C.M. Wilson, Prompt neutrons from photofission and its use in homeland security applications, in: 2010 IEEE International Conference on Technologies for Homeland Security (HST), Waltham, MA, 2010, pp. 379–384, http://dx.doi.org/10.1109/THS.2010.5654938.
[5] M.M. Bourne, S.D. Clarke, M. Paff, A. DiFulvio, M. Norsworthy, S.A. Pozzi, Digital pile-up rejection for plutonium experiments with solution-grown stilbene, Nucl. Instrum. Methods Phys. Res. A 842 (2017) 1–6.
[6] Kui-Nian Li, Xian-Peng Zhang, Qiang Gui, Peng Jin, Geng Tian, Characterization of the new scintillator Cs2LiYCl6:Ce3+, Nucl. Sci. Tech. 29 (2018) 11.
[7] H. Arahmane, A. Mahmoudi, E.-M. Hamzaoui, Y.B. Maissa, R.C. El Moursli, Neutron-gamma discrimination based on support vector machine combined to nonnegative matrix factorization and continuous wavelet transform, Measurement 149 (2020) 106958.
[8] E. Ronchi, P.-A. Soderstrom, J. Nyberg, E.A. Sunden, S. Conroy, G. Ericsson, C. Hellesen, M. GatuJohnson, M. Weiszflog, An artificial neural network based neutron–gamma discrimination and pile-up rejection framework for the BC-501 liquid scintillation detector, Nucl. Instrum. Methods Phys. Res. A 610 (2009) 534–539.
[9] P.-A. Söderström, G. Jaworski, J.J.V. Dobón, J. Nyberg, J. Agramunt, G. de Angelis, S. Carturan, J. Egea, M.N. Erduran, S. Ertürk, G. de France, A. Gadea, A. Goasduff, V. González, K. Hadyńska-Kle, T. Hüyük, V. Modamio, M. Moszynski, A. Di Nitto, M. Palacz, N. Pietralla, E. Sanchis, D. Testov, A. Triossi, R. Wadsworth, Neutron detection and gamma-ray suppression using artificial neural networks with the liquid scintillators BC-501a and BC-537, Nucl. Instrum. Methods Phys. Res. A 916 (2019) 238–245.
[10] G. Liu, M.D. Aspinall, X. Ma, M.J. Joyce, An investigation of the digital discrimination of neutrons and γ rays with organic scintillation detectors using an artificial neural network, Nucl. Instrum. Methods Phys. Res. A 607 (2009) 620–628.
[11] T. Alharbi, Principal component analysis for pulse shape discrimination of scintillation radiation detectors, Nucl. Instrum. Methods Phys. Res. A 806 (2016) 240–243.
[12] C. Fu, A. Di Fulvio, S.D. Clarke, D. Wentzloff, S.A. Pozzi, H.S. Kim, Artificial neural network algorithms for pulse shape discrimination and recovery of piled-up pulses in organic scintillators, Ann. Nucl. Energy 120 (2018) 410–421.
[13] Xianfei Wen, Andreas Enqvist, Pulse shape discrimination of Cs2LiYCl6:Ce3+ detectors at high count rate based on triangular and trapezoidal filters, Nucl. Instrum. Methods Phys. Res. A 866 (2017) 129–133.
[14] J. Griffiths, S. Kleinegesse, D. Saunders, R. Taylor, A. Vacheret, Pulse shape discrimination and exploration of scintillation signals using convolutional neural networks, Mach. Learn.: Sci. Technol. 1 (2020) 045022.
[15] Y. LeCun, Y. Bengio, G. Hinton, Deep learning, Nature 521 (2015) 436–444.
[16] A.Y. Hannun, P. Rajpurkar, M. Haghpanahi, G.H. Tison, C. Bourn, M.P. Turakhia, A.Y. Ng, Cardiologist-level arrhythmia detection and classification in ambulatory electrocardiograms using a deep neural network, Nat. Med. 25 (2019) 65–69.

[17] A. Dutta, K.E. Holbert, Discrimination of neutron-Gamma ray pulses with pileup using normalized cross correlation and principal component analysis, IEEE Trans. Nucl. Sci. 63 (6) (2016) 2764–2771.
[18] E.V.D. Van Loef, P. Dorenbos, C.W.E. Van Eijk, K.W. Kramer, H.U. Gudel, J. Phys. Condens. Mat. 14 (2002) 8481.
[19] R. Brun, F. Rademakers, Root - an object oriented data analysis framework, proceedings aihenp'96 workshop, lausanne, sep. 1996, Nucl. Instrum. Methods Phys. Res. A 389 (1997) 81–86.
[20] Z. Wang, J. Zeng, T. Zhu, Y. Wang, C. Yang, R. Zhou, Optimization of integration limit in the charge comparison method based on signal shape function, Nucl. Instrum. Methods Phys. Res. A 760 (2014) 5–9.
[21] J. Zhang, M.E. Moore, Z. Wang, R. Zhou, C. Yang, J.P. Hayward, Study of sampling rate influence on neutron–gamma discrimination with stilbene coupled to a silicon photomultiplier, Appl. Radiat. Isot. 128 (2017) 120–124.
[22] B.S. McDonald, M.J. Myjak, M.A. Zalavadia, J.E. Smart, J.A. Willett, P.C. Landgren, C.R. Greulich, A wearable sensor based on CLYC scintillators, Nucl. Instrum. Methods Phys. Res. A 821 (2016) 73.
[23] N. Blasi, S. Brambilla, F. Camera, S. Ceruti, A. Giaz, L. Gini, F. Groppi, S. Manenti, A. Mentana, B. Million, S. Riboldia, Fast neutron detection efficiency of 6Li and 7Li enriched CLYC scintillators using an Am-Be source, J. Instrum. 13 (2018) P11010.
[24] F. Chollet, et al., Keras: Deep learning for humans, GitHub Repos (2015) https://keras.io/.